Idealized Large-Eddy Simulations of Stratocumulus Advecting over Cold Water. Part I: Boundary Layer Decoupling

YOUTONG ZHENG,[a] HAIPENG ZHANG,[a] DANIEL ROSENFELD,[b] SEOUNG-SOO LEE,[a] TIANNING SU,[a] and ZHANQING LI[a]

[a] *Earth System Science Interdisciplinary Center, University of Maryland, College Park, College Park, Maryland*
[b] *Hebrew University of Jerusalem, Jerusalem, Israel*

(Manuscript received 20 April 2021, in final form 12 October 2021)

ABSTRACT: We explore the decoupling physics of a stratocumulus-topped boundary layer (STBL) moving over cooler water, a situation mimicking warm-air advection (WADV). We simulate an initially well-mixed STBL over a doubly periodic domain with the sea surface temperature decreasing linearly over time using the System for Atmospheric Modeling large-eddy model. Due to the surface cooling, the STBL becomes increasingly stably stratified, manifested as a near-surface temperature inversion topped by a well-mixed cloud-containing layer. Unlike the stably stratified STBL in cold-air advection (CADV) that is characterized by cumulus coupling, the stratocumulus deck in the WADV is unambiguously decoupled from the sea surface, manifested as weakly negative buoyancy flux throughout the subcloud layer. Without the influxes of buoyancy from the surface, the convective circulation in the well-mixed cloud-containing layer is driven by cloud-top radiative cooling. In such a regime, the downdrafts propel the circulation, in contrast to that in CADV regime for which the cumulus updrafts play a more determinant role. Such a contrast in convection regime explains the difference in many aspects of the STBLs including the entrainment rate, cloud homogeneity, vertical exchanges of heat and moisture, and lifetime of the stratocumulus deck, with the last being subject to a more thorough investigation in Part II. Finally, we investigate under what conditions a secondary stratus near the surface (or fog) can form in the WADV. We found that weaker subsidence favors the formation of fog whereas a more rapid surface cooling rate does not.

SIGNIFICANT STATEMENT: The low-lying blanketlike clouds, called stratocumulus (Sc), reflect much incoming sunlight, substantially modulating Earth's temperature. While much is known about how the Sc evolves when it moves over warmer water, few studies examine the opposite situation of Sc moving over colder water. We used a high-resolution numerical model to simulate such a case. When moving over cold water, the Sc becomes unambiguously decoupled from the water surface, distinctive from its warm counterpart in which the Sc interacts with the water surface via intermittent cauliflower-like clouds called cumulus clouds. Such decoupling influences many aspects of the Sc–sea surface system, which combine to alter the ability of the Sc to reflect sunlight, thereby influencing the climate. This work laid the foundation for future work that quantifies the contribution of such a decoupled Sc regime to Earth's radiative budget and climate change.

KEYWORDS: Clouds; Turbulence; Boundary layer; Thermodynamics; Large eddy simulations

1. Introduction

Marine stratocumulus (Sc) significantly alters Earth's radiative budgets at both the surface and the top of the atmosphere (Hartmann et al. 1992; Hahn and Warren 2007; Wood 2012). The Sc strongly interacts with the sea surface via exchanges of heat, moisture, and momentum, forming a coupled Sc–surface system commonly known as the stratocumulus-topped planetary boundary layer (STBL). The earliest credible description of the STBL physics is Lilly's (1968) mixed-layer model. The model treats the column of air from the surface to the top of Sc as a well-mixed bulk layer and parameterizes basic cloud physics and fluxes (i.e., energy, moisture, and mass). The model succeeds in explaining a series of important behaviors of STBL over the subtropical oceans such as the STBL response to large-scale environment (Schubert et al. 1979a,b; Wakefield and Schubert 1981; Stevens 2006), the STBL decoupling during the cloud regime transition (Bretherton and Wyant 1997; Zheng et al. 2020), diurnal cycle (Caldwell et al. 2005; Zhang et al. 2005), dominant time scales (Jones et al. 2014), slow manifold behavior (Bretherton et al. 2010), and aerosol influences on Sc (Wood 2007; Caldwell and Bretherton 2009; Uchida et al. 2010).

The mixed-layer model becomes invalid if the STBL stably stratifies, a phenomenon widely known as STBL decoupling (Nicholls 1984). The decoupling physics can be understood from the perspective of boundary layer energetics. In a well-mixed STBL over cold water, air parcels entrained from the overlying inversion are cooled by thermal radiation at the cloud top, sinking through the boundary layer. This well-mixed state is sustained by a rough balance between entrainment warming and radiative cooling in the upper part of the STBL. When the warming outweighs the cooling, the

Supplemental information related to this paper is available at the Journals Online website: https://doi.org/10.1175/JAS-D-21-0108.s1.

Zheng's current affiliations: Program in Atmospheric and Oceanic Sciences, Princeton University, and NOAA/Geophysical Fluid Dynamics Laboratory, Princeton, New Jersey.

Corresponding author: Youtong Zheng, yz1799@princeton.edu

DOI: 10.1175/JAS-D-21-0108.1

© 2021 American Meteorological Society. For information regarding reuse of this content and general copyright information, consult the AMS Copyright Policy (www.ametsoc.org/PUBSReuseLicenses).

Brought to you by PRINCETON UNIVERSITY LIBRARY | Unauthenticated | Downloaded 07/29/22 03:00 PM UTC

entrained warm air parcels are too light to sink, leading to the stable stratification of the boundary layer. Examples include the decoupling during the subtropical stratocumulus-to-cumulus transition due to enhanced entrainment warming (Bretherton and Wyant 1997), decoupling by precipitation that warms the cloud layer (Nicholls 1984; Stevens et al. 1998), and daytime decoupling by solar insolation that weakens cloud-top radiative cooling (Nicholls and Leighton 1986; Zheng et al. 2018).

The above decoupling mechanisms have been studied in subtropical conditions where the trade winds advect the STBL toward the equator with warmer surfaces. The cold-air advection builds up the potential energy of the environment so that the decoupled STBLs are typically conditionally unstable. This allows for the development of cumulus (Cu) that often penetrates the Sc decks, forming Cu-coupled STBLs. In such a cloud regime, the Sc can interact with the surface through the conduits of the Cu convection so that whether or not to call the boundary layer "decoupled" has been controversial (Miller and Albrecht 1995; Stevens et al. 1998; Goren et al. 2018; Zheng et al. 2018; Zheng and Li 2019).

To reconcile the controversy, Zheng et al. (2020) added a new dimension, namely, low-level temperature advection, to the problem. Zheng et al. (2020) considered the coupling state of STBL in a spectrum of low-level temperature advection ranging from the extremely cold-air advection such as cold-air outbreaks to the warm-air advection in the warm sector of midlatitude cyclones. The STBLs embedded in cold-air advection flows are either fully coupled (i.e., well mixed) or Cu coupled. The unambiguously decoupled STBLs predominantly occur in warm-air advection conditions where the stable stratification is sufficiently strong to prohibit the cumulus coupling. This view is supported by ground-based observations from the Southern Ocean, northeast subtropical Pacific, and northeast Atlantic (Zheng et al. 2020). These observations show that, as the low-level flow shifts from cold to warm-air advection, the boundary layer turns from a Cu-coupled STBL to a considerably stably stratified STBL without Cu coupling (i.e., unambiguously decoupled STBL) (see the schematic diagram of Fig. 4 in Zheng et al. 2020).

Poorly understood is the unambiguously decoupled STBLs experiencing warm advection. In contrast to Cu-coupled STBLs, typical at subtropics, the STBLs under warm advection conditions receive scarce attention despite their potential abundance in midlatitudes[1] (Agee 1987; Fletcher et al. 2016; Wall et al. 2017; Scott et al. 2020). This motivates the current study. In addition to testing the hypothesis that unambiguously decoupled STBLs are more likely to occur in warm-air advection conditions than the cold ones, we aim to elucidate the physics of STBL response to warm advection using idealized large-eddy simulations. By the "idealized," we mean simulating an STBL over a doubly periodic domain with the sea surface temperature (SST) decreasing over time to mimic the influences of warm-air advection. This idealized setup is the same as the conventional LES studies of Sc-to-Cu transitions (Sandu and Stevens 2011; Van der Dussen et al. 2013; Bretherton and Blossey 2014), in which the SST increases over time. Such consistency allows for direct comparisons.

In addition to further the understanding of decoupling dynamics, another motivation is a lack of consensus on the role of horizontal temperature advection on low cloud radiative effects. Prior observations show that marine low clouds are considerably fewer and thinner under warmer air advection conditions (Norris and Iacobellis 2005; Myers and Norris 2015; Klein et al. 2017; Scott et al. 2020). Their interpretation is that the warm-advection-induced decoupling leads to less moisture supply from the sea surface to the clouds, thereby thinning the clouds. Contrasting pieces of evidence, however, exist. For example, Zheng and Li (2019) found that clouds can be very persistent even if they are decoupled from the sea surface under warm advection conditions, as shown by geostationary satellite images and ship-based remote sensing data. This finding is consistent with Goren et al. (2018), who found that precipitating marine clouds are more persistent in decoupled STBLs than coupled ones. Moreover, some studies show no statistically significant dependence of low cloud radiative effects on temperature advection in climate models (D. McCoy 2020, personal communications) and ground-based observations over midlatitude oceans (Naud et al. 2020). The mixed lines of evidence suggest a lack of understanding of the mechanism underlying the low-cloud response to warm-air advection.

In summary, this two-part study attempts to elucidate the physical mechanisms of warm-advection-induced decoupling (Part I) and its control on low-cloud radiative effects (Zhang et al. 2021, manuscript submitted to *J. Atmos. Sci.*, hereafter Part II) by using idealized large-eddy simulations. Part I is dedicated to decoupling dynamics whereas Part II focuses on its implications for the low cloud feedback. Although the warm-air advection is our focus, our analyses are centered on comparing the results of warm-air advection with the cold-air advection (as the benchmark). This enables a clearer presentation of the new insights in the context of conventional knowledge. The next section introduces the LES model and the experiments. Section 3 shows the results, followed by the discussion and concluding remarks.

2. Large-eddy simulations

a. Model and case descriptions

We use the System for Atmospheric Modeling (SAM) model, version 6.11.3 (Khairoutdinov and Randall 2003). SAM uses liquid water static energy (h_l), total nonprecipitating water mixing ratio (q_t), and total precipitating water mixing ratio as prognostic thermodynamic scalars. We use the advection scheme developed by Smolarkiewicz and Grabowski (1990), the 1.5-order prognostic subgrid-scale model, a simplified (drizzle only) version of Khairoutdinov and Kogan's (2000) microphysics scheme and RRTMG radiation

[1] Zheng et al. (2020) reported that stratocumulus clouds experiencing warm-air advection occupy more than 25% of the samples of single-layer stratocumulus collected during two midlatitude field campaigns.

Brought to you by PRINCETON UNIVERSITY LIBRARY | Unauthenticated | Downloaded 07/29/22 03:00 PM UTC

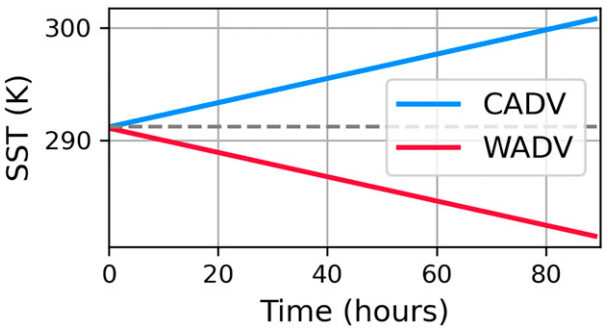


FIG. 1. Time evolution of the sea surface temperature in the two simulations.

(Iacono et al. 2008). Surface fluxes of temperature, moisture, and momentum are calculated by similarity theory.

We use a horizontal grid spacing of 35 m in a doubly periodic domain with a size of 4200^2 m^2. We chose such a small domain size purely for computational efficiency. It should be too small to represent mesoscale convective circulation typical for precipitating STBLs. The STBLs studied here are weakly precipitating so that the influence of mesoscale dynamics should be minor. This is confirmed by a sensitivity test for a larger domain of 8400^2 m^2 that yields nearly identical results (see the online supplementary material). The vertical grid spacing is set as 5 m in the cloud and inversion layer to resolve entrainment. The grid spacing stretches above ~2400 m until the domain top of ~4200 m, which is high enough for gravity wave damping. There is a total of 512 vertical grids. Previous studies suggest that the LES-simulated entrainment is less realistic for coarse vertical grids (Mellado 2017; Mellado et al. 2018). To examine whether a vertical grid spacing of 5 m is enough, we conduct a sensitivity test by changing the vertical grid size from 5 to 3 m, showing little sensitivities (supplementary material).

The base case for our simulations is the case from the Atlantic Stratocumulus Transition Experiment (ASTEX) (Albrecht et al. 1995). The ASTEX case has been a benchmark for LESs of the Sc-to-Cu transitions (Van der Dussen et al. 2013). The initial profiles are shown in the supplementary material. A unique aspect of the ASTEX case is that observations from an aircraft and balloons are "Lagrangian" for they follow the evolution of STBL air mass. This is particularly important for simulating the STBL response to horizontal temperature advection, for which the SST evolution along the airmass trajectory is the key driver. During the ASTEX, the SST increases by ~4 K over the 40-h simulation of the ASTEX case. Such an increase in SST is widely regarded as the determinant driver of the cloud regime transition.

As stated in the introduction, we use a cold-air advection case as a benchmark for understanding the role of warm advection. To that end, we conduct two idealized experiments by simplifying the forcing of the original ASTEX case (Fig. 1). In the first experiment, we linearize the SST increase rate, yielding an SST increasing rate of 2.6 K day^{-1} (named "CADV"). The linearized CADV case well reproduces the evolution of the original ASTEX case [see Fig. 1 in Zheng et al. (2021)]. In the second experiment, we decrease the SST by 2.6 K day^{-1} to mimic the influence of warm-air advection (named "WADV"). To remove the influence of diurnal cycle, we set the solar zenith angle as the diurnal average of 68.72°. All other initial and forcing conditions are the same (Van der Dussen et al. 2013).

The WADV run is highly idealized. In the real world, the low-level horizontal temperature advection strongly couples with other synoptic variables. For example, warm-air advection is typically coincident with large-scale ascent motions whereas cold-air advection is more likely to occur in a subsiding atmosphere (Holton 1973; Norris and Klein 2000; Zheng et al. 2020). In that regard, it is unrealistic that the CADV and WADV start with the same initial conditions and experience the same large-scale forcing. But the purpose of this study is not to reproduce the real-world STBLs, but to understand the most essential physics behind the problem. All the existing hypotheses for STBL response to warm-air advection are centered on the stabilization effect of warm advection as the most determinant process (Norris and Iacobellis 2005; Klein et al. 2017; Scott et al. 2020). In other words, our current level of understanding does not allow for formulating a hypothesis sophisticated enough to account for every aspect of the problem. Thus, we consider our simulations a starting point for future more realistic numerical explorations.

b. Diagnostic statistics

The boundary layer height (z_i) and heights of capping inversion base (z_i^-) and top (z_i^+) are determined using the method developed by Yamaguchi and Randall (2008) that is based on the profile of h_l variance ($\overline{h_l'^2}$):

$$z_i^+ = z, \quad \text{where } \overline{h_l'^2} = 0.05 \times \max\left(\overline{h_l'^2}\right) \text{ and } z > z_{\max}, \quad (1a)$$

$$z_i^- = z, \quad \text{where } \overline{h_l'^2} = 0.05 \times \max\left(\overline{h_l'^2}\right) \text{ and } z < z_{\max}, \quad (1b)$$

and $z_{\max}$ is defined as $z_{\max} = z$, where $\overline{h_l'^2} = \max\left(\overline{h_l'^2}\right)$.

With the z_i^- and z_i^+, we can compute the buoyancy jump across the inversion, which will be used to quantify the entrainment-driven decoupling shown later. We quantify the degree of stratification of an STBL using the h_l averaged over the top 10% of the z_i minus the h_l averaged over the bottom 10% of the z_i, marked as $\Delta_{\mathrm{BL}} h_l$.

We determine the lifting condensation level (LCL) using the exact analytic formula developed by Romps (2017). The entrainment rate (w_e) is determined using the boundary layer mass budget equation: $w_e = dz_i/dt - w_{\mathrm{sub}}$, in which the w_{sub} is the large-scale subsidence rate at the boundary layer top.

3. Results

a. Time evolution

Figures 2 and 3 show the time evolution of selected outputs, which illustrate many characteristics of the STBL under the

Brought to you by PRINCETON UNIVERSITY LIBRARY | Unauthenticated | Downloaded 07/29/22 03:00 PM UTC

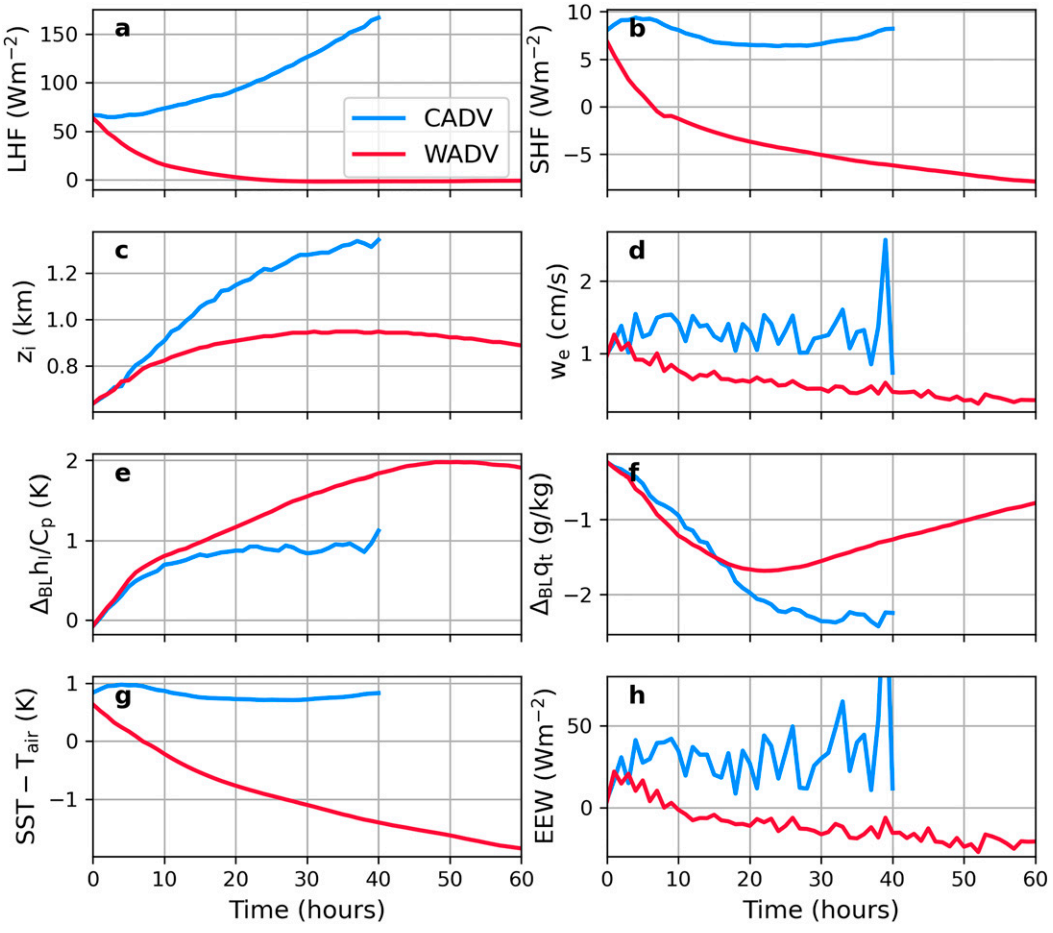


FIG. 2. Time series of key variables of experiments CADV (blue) and WADV (red): (a) surface latent heat flux, (b) surface sensible heat flux, (c) main inversion height, (d) entrainment rate, (e) $\Delta_{BL}h_l/c_p$, (f) $\Delta_{BL}q_t$, (g) sea surface temperature minus near-surface air temperature, and (h) EEW [Eq. (2)].

influence of warm-air advection. The warm-air advection substantially suppresses the surface latent and sensible heat fluxes (Figs. 2a,b). This lowers the turbulence level of the boundary layer, weakens the entrainment near the boundary layer top (Fig. 2d), and slows the deepening (or even shallowing) of the boundary layer (Fig. 2c). Such a contrast in surface fluxes, as will be evident later, is the most essential factor explaining most of the differences between the two simulations.

Figures 3a and 3b show the time–height plots of the cloud fraction for the two runs. The CADV presents a textbook-like Sc-to-Cu transition whereas the WADV shows a solid Sc deck persistent throughout the simulation. The persistence is primarily due to the weak entrainment drying, discussed in detail in Part II. Because the focus of this study is the boundary layer decoupling, we look at time evolution of h_l and q_t profiles (Figs. 3c–f). Both regimes show increasingly stably stratified boundary layers, but their geometries of stratification differ greatly, which can be more clearly seen from the sounding at a selected time of $t = 30$ h (Fig. 4). In CADV, the boundary layer is stratified into two well-mixed layers: the upper cloud-containing layer driven by radiative cooling and the bottom layer driven by surface heating. These two layers are separated by a weakly stratified layer. In WADV, however, the stratification concentrates near the surface, as seen from a well-defined temperature inversion in the lowest quarter of the boundary layer. Above the inversion is a well-mixed cloud-containing layer. The convection in this mixed layer is driven by cloud-top radiative cooling, suggested by the top-heavy structure of vertical velocity variance (Figs. 3h and 4c) and the negative vertical velocity skewness (Fig. 3j), an indicator of top-driven convection (Moeng and Rotunno 1990).

The above analysis dictates two different decoupling mechanisms: entrainment-warming-driven decoupling in CADV and surface-cooling-driven decoupling in WADV. This statement can be demonstrated by quantifying the role of entrainment warming in decoupling. Here we use a model diagnostic called "excess entrainment warming" (EEW), developed by Zheng et al. (2021). The EEW is defined as

$$\mathrm{EEW} = \underbrace{\rho C_p w_e \Delta_{\mathrm{inv}} \theta_v}_{\Delta\text{Entrainment warming}} + \underbrace{\Delta_{\mathrm{cld}} F_{\mathrm{rad}} + \rho L_v \Delta_{\mathrm{cld}} F_{\mathrm{prec}}}_{\Delta\text{Diabatic cooling}}, \qquad (2)$$

Brought to you by PRINCETON UNIVERSITY LIBRARY | Unauthenticated | Downloaded 07/29/22 03:00 PM UTC

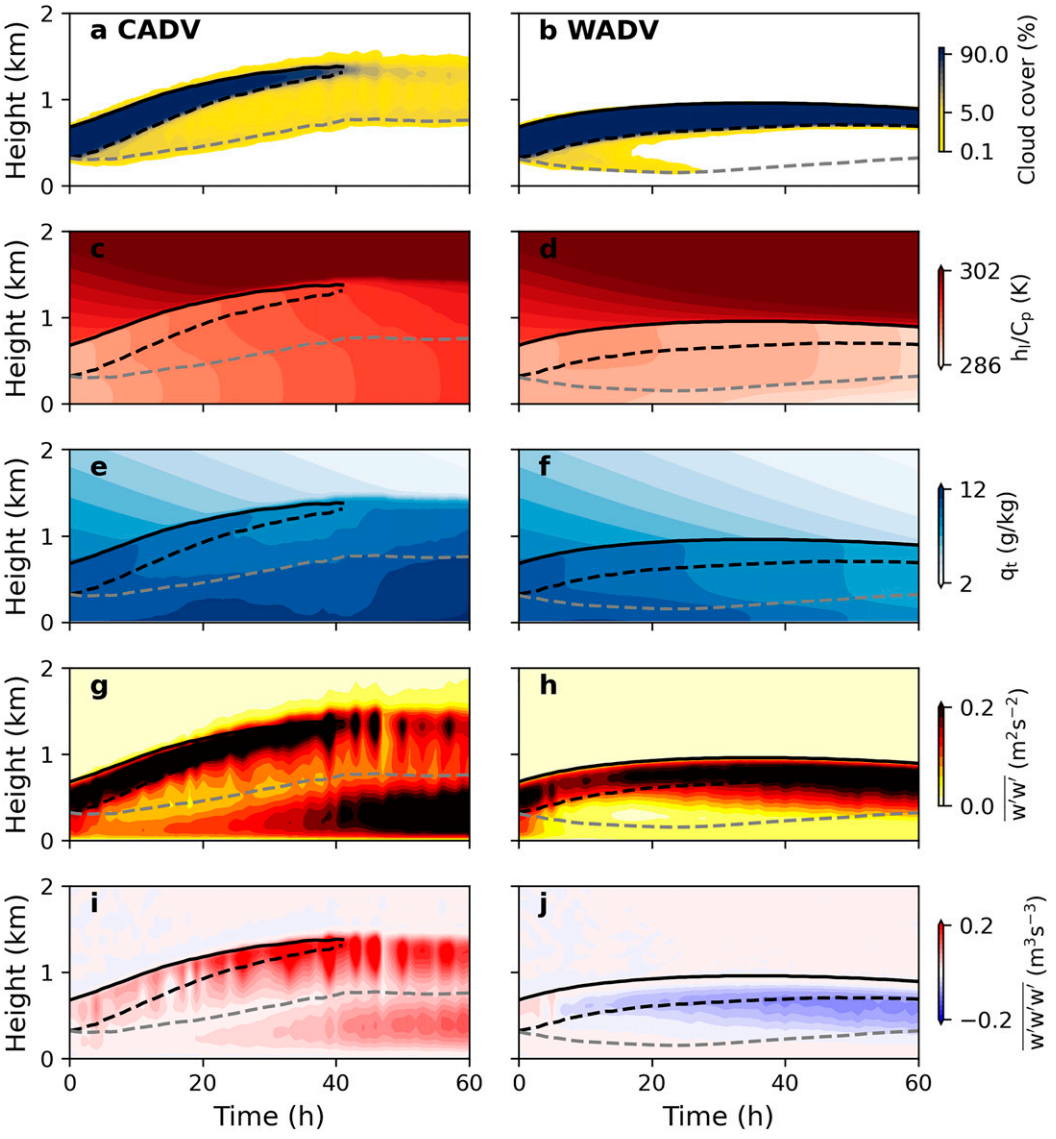


FIG. 3. Time–height plots of key variables of experiments (left) CADV and (right) WADV. The black solid line, black dashed line, and gray dashed line are cloud-top height, cloud-base height, and lifting condensation level, respectively.

where ρ is the air density, C_p is the specific heat of air, L_v is the latent heat of evaporation of water, F_{rad} is the radiative flux (W m^{-2}), and F_{prec} is the precipitation flux (m^{-1}). The symbols Δ_{inv} and Δ_{cld} represent the changes (top minus bottom) across the capping inversion and Sc cloud layer, respectively. A larger EEW means that the diabatic cooling (radiative cooling compromised by the precipitation-induced heating in the cloud layer) is not sufficient to balance the entrainment warming so that the entrained air is not cold enough to be sink through the subcloud layer. This causes the accumulation of warm air in the upper boundary layer, stably stratifying the STBL. A small or even negative value means that the entrainment-induced warming is balanced by the diabatic cooling, preventing the decoupling. Figure 2h shows the evolution of EEW for the two experiments. The CADV has an EEW of several tens of watts per square meter throughout the simulation, meaning that entrainment warming considerably outweighs the diabatic cooling. On the contrary, the EEW remains negative most of the time in WADV, demonstrating a minimal role of entrainment in the decoupling. Such a contrasting role of entrainment in the decoupling is more directly seen from the evolutions of the three components of the EEW (Fig. 5).

Given that the entrainment cannot explain the decoupling in WADV, the near-surface cooling is the dominant decoupling factor. To understand what drives the near-surface cooling in WADV, we analyze the budgets of dh_l/dt in the lowest 200 m when the cooling is most distinctive. We found that the

Brought to you by PRINCETON UNIVERSITY LIBRARY | Unauthenticated | Downloaded 07/29/22 03:00 PM UTC

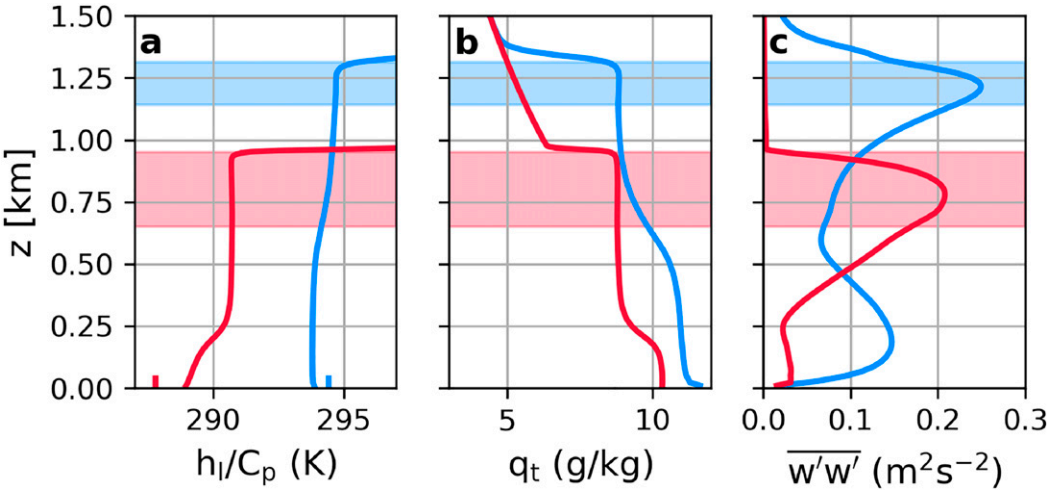


FIG. 4. Profiles of (a) h_l/C_p, (b) q_t, and (c) vertical velocity variance for CADV (blue) and WADV (red) at $t = 30$ h. Ticks at the bottom of (a) are the sea surface temperatures.

turbulent transport, $(dh_l/dt)_{\text{tur}}$, and radiation, $(dh_l/dt)_{\text{rad}}$, are the dominant controllers, which are illustrated in Fig. 6. The cooling effect of turbulent transport is straightforward to understand. In WADV, except at the beginning, boundary layer air is notably warmer than the SST (Fig. 2g), leading to the downward loss of heat to the sea surface. This causes cooling of the bottom boundary layer. However, turbulent transport is not the only cooling mechanism, as seen from the thin layer of turbulent warming in the lowest few tens of meters (Fig. 6b).

The thin layer of turbulent warming can be explained by the turbulence adjustment to the near-surface radiative cooling (Fig. 6c). What causes the abnormally large radiative cooling near the surface? According to the conventional knowledge about radiative transfer, we know that atmospheric radiative cooling has three contributing components: 1) exchange of radiative energy with underlying atmosphere, 2) exchange of radiative energy with overlying atmosphere, and 3) radiative energy escaping to space. In a typical atmosphere where temperature decreases with altitude, the first two components roughly cancel each other, leaving the "cooling-to-space" component the dominant one (Petty 2006). This is not the case here for the air near the surface: both the overlying and underlying air masses are cooler (Fig. 4a). Thus, exchanges of radiative energy in both directions cause loss of energy, considerably increasing the radiative cooling. Such a local cooling induces local convergence of turbulent flux as an adjustment process (Edwards 2009).

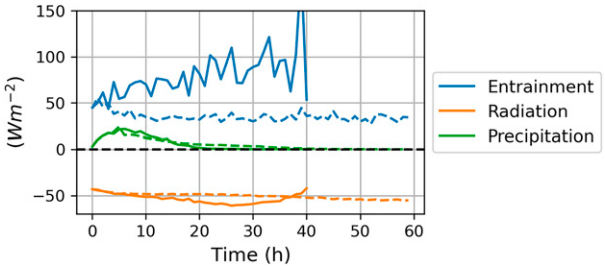


FIG. 5. Time series of the three EEW components in CADV (solid) and WADV (dashed).

The aggregate role of the radiation and turbulence, $(dh_l/dt)_{\text{tur}+\text{rad}}$, is a cooling effect. The $(dh_l/dt)_{\text{tur}+\text{rad}}$ (Fig. 6d) bears a similarity with the dh_l/dt (Fig. 6a), suggesting that the two processes can explain the bulk of the near-surface cooling. The remaining difference is due to the precipitation and large-scale transport, which play a secondary role.

In summary, the stable stratifications of STBLs in CADV and WADV are explained by entrainment-induced warming and near-surface cooling (by turbulence and radiation), respectively. These two decoupling mechanisms can be conceptualized into a decoupling dipole: top-warming-driven versus bottom-cooling-driven decoupling.

b. *The already decoupled phase*

We have discussed processes leading to the decoupling in both regimes. Now we characterize the turbulent properties of STBLs in their already decoupled phases. Strictly speaking, there is no such thing as an equilibrium phase in our simulations because the SST keeps evolving and the STBL keeps responding. Here, we take model outputs at $t = 30$ h as representations of already decoupled STBLs for the two regimes. One justification for selecting $t = 30$ h is that the stratification degree at CADV already saturates at $t = 30$ h, suggesting a quasi-equilibrium state (Fig. 2e). In WADV, the STBL is still stratifying, but the qualitative characteristics of the STBL (e.g., thermodynamic structure, turbulence, and cloud properties) remain similar throughout the simulations. Selecting different times of the WADV run does not influence the main conclusion of this paper.

We first look at the three-dimensional (3D) visualization of the STBLs at $t = 30$ h (Fig. 7). To more clearly visualize the cloud–surface decoupling, we show the surface plots of the near-surface q_t, defined as the top 1% of q_t in the vertical

Brought to you by PRINCETON UNIVERSITY LIBRARY | Unauthenticated | Downloaded 07/29/22 03:00 PM UTC

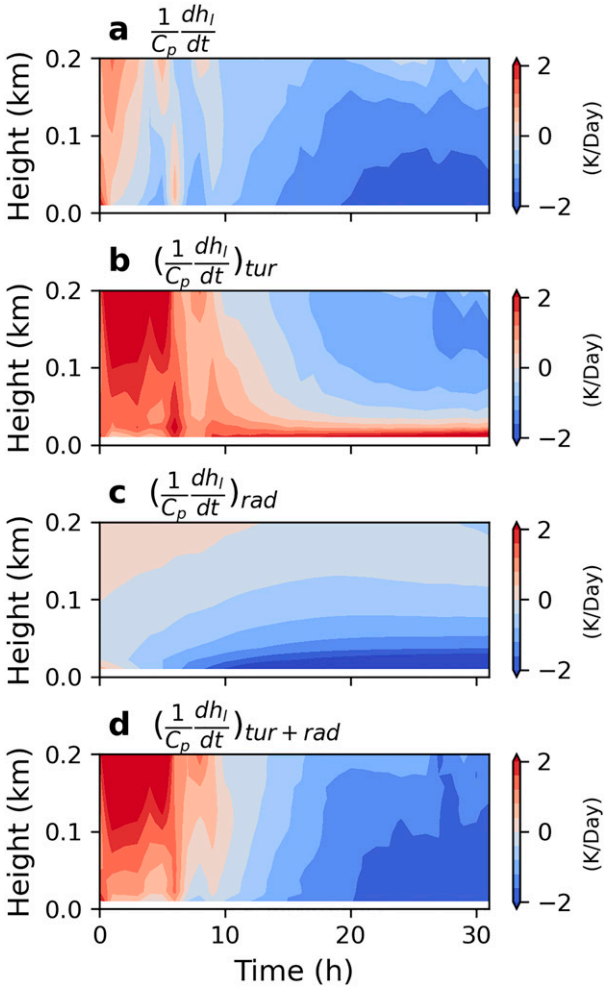


FIG. 6. Time–height plots of (a) total heating rate, (b) heating rate due to turbulence, (c) heating rate due to radiation, and (d) heating rate due to turbulence and radiation for WADV.

(dark red surface). The CADV regime is characterized by intermittent Cu clouds penetrating the Sc deck, known as the Cu-coupled STBL. The contour of the near-surface q_t extends vertically from the surface to the base of Cu. Through the conduit of Cu, the water from the sea surface feeds into the Sc deck. Such a feeding effect is absent in WADV. In WADV, there is only a single layer of solid Sc deck, completely separate from the surface humid air trapped near the surface. We provide movies of 2D fluid visualization for the two runs to aid in intuitively understanding the results (see animations 1 and 2 in the supplemental material).

Such a difference in the cloud–surface interaction is augmented by vertical velocity fields at different levels. Figure 8 shows the vertical velocity at $z = 10$ m (left), $z = 0.5z_b$ (center), and $z = z_b$ (right). The turbulent flow near the surface of the CADV regime is relatively elongated, consistent with the typical flow structure in convective boundary layers (Moeng and Rotunno 1990). In WADV, however, the flow is more random with a less evident elongated pattern, typical for stratified flows (Mahrt 2014). At $z = 0.5z_b$ in the CADV, small patches of isolated updrafts (blobs of red colors) start to emerge. These updraft regions are more humid than the surrounding regions. This pattern resembles the typical "cumulus-like" convection: moist, narrow, and strong updrafts surrounded by drier, wider, and weaker subsidence (Bjerknes 1938). This is further supported by the positive skewness of vertical velocity, characteristic of surface-driven convection (Fig. 8h). In WADV, however, the "cumulus-like" convection is absent, as seen from a lack of concentrated updrafts. The skewness of vertical velocity is negative (Fig. 8h), suggesting a dominance of top-cooling-driven turbulence (Wyngaard 1987; Moeng and Rotunno 1990). Such a contrast in turbulence regime persists at $z = z_b$.

The flow visualizations (Figs. 7 and 8) suggest two distinctive convection regimes: surface-heating-driven cumulus-like convection for CADV versus top-cooling-driven stratocumulus-like convection for WADV. Such a difference can be more directly seen by conditionally sampling the parcels in rising ($w > 0$) and sinking motions ($w < 0$) (Fig. 9a). Figure 8a shows that the vertical velocity variance is considerably stronger for updrafts than downdrafts in CADV, suggesting a more determinant role of updrafts in driving the vertical mixing, whereas the opposite is true for WADV. Note that the cloud-top radiative cooling still contributes to driving the convection in the CADV, as seen from the local maxima of vertical velocity variance in the upper Sc layer. But even in such a Sc layer, the updrafts contribute more to the turbulence via penetration of the Cu convection.

The relative strength of updrafts and downdrafts makes a substantial difference to how heat and moisture are transported in the vertical (Figs. 9b,c). In CADV, the vertical transport of moisture is realized by updrafts that carry humidity from the sea surface upward, feeding the Sc deck (Fig. 9b). In contrast, in the WADV, the downdrafts play a more dominant role in the vertical exchange of moisture: downdrafts transport entrained dry air toward the surface. At $z = z_b$ of WADV, the supply of moisture via updrafts is close to zero, meaning that the Sc deck almost entirely decouples from the source of humidity from below.

A similar conclusion can be drawn from the heat flux (Fig. 9c). The heat flux profile is relatively more complex due to the influences of diabatic heating/cooling (i.e., radiation and precipitation) to which the turbulent flux must adjust (Stevens et al. 1998). Hence we focus on the subcloud layer where the diabatic heating/cooling is minimal. Both regimes show a downward transport of heat, but the transport in CADV is realized by updrafts, whereas, in WADV, the downdrafts drive the downward transports of warm entrained air.

In addition to the profiles of heat and moisture fluxes, it is informative to look at the buoyancy flux that dictates boundary layer energetics (Fig. 9d). In CADV, the buoyancy flux is mostly positive except near the LCL. Such a structure of buoyancy profile is consistent with the conventional wisdom based on the argument of hypothetical parcel trajectory [see Bretherton (1997) for details]. Again, the updrafts dominate the positive buoyant flux (less dense air rises), converting the potential energy of the environment to turbulent kinetic energy. Such a large buoyancy flux for updrafts is largely

Brought to you by PRINCETON UNIVERSITY LIBRARY | Unauthenticated | Downloaded 07/29/22 03:00 PM UTC

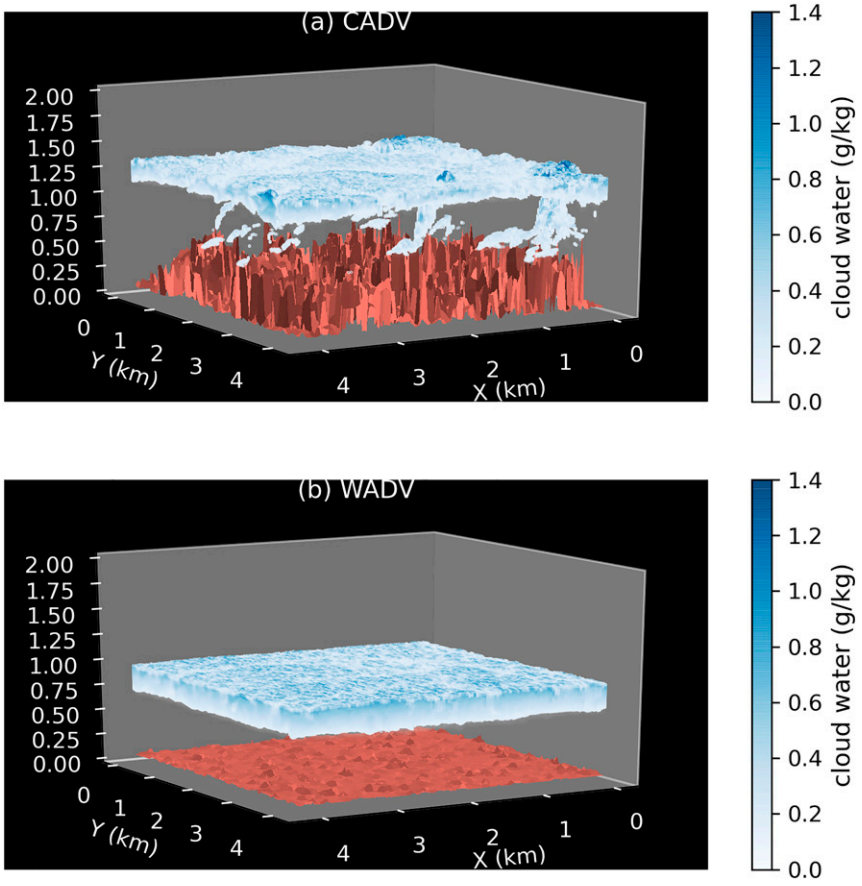


FIG. 7. Three-dimensional visualizations of cloud liquid water content at $t = 30$ h for the (a) CADV and (b) WADV experiments. The red surfaces are the contours of the top 1% q_t in each column.

contributed by the water vapor. As seen in Fig. 9c, the heat flux for updrafts is negative throughout most of the boundary layer, which suggests cooler air ascending. The buoyancy of the ascending cool air stems from the concentration of water vapor, as seen from the strong q_t flux in updrafts (Fig. 9b). In WADV, however, the cloud layer and subcloud layer exhibit opposite signs. In the cloud layer, the buoyancy flux is positive, contributed by both updrafts and downdrafts through latent heating and diabatic cooling, respectively. The downdrafts, again, contribute more. In the subcloud layer, the buoyancy flux is slightly negative. Such a dipole-like geometry of buoyancy flux profile resembles that of the heat flux (Fig. 9c), suggesting the contribution of buoyancy from water vapor is insignificant, especially in the subcloud layer.

So what drives the downward motion of the warm air if the water vapor effect does not contribute? From the perspective of the heat budget constraint, the warm air must descend somewhere in the subcloud layer in order to transfer heat from the atmosphere into the sea surface, a necessary consequence of WADV (warm air overlying cold surface). Then what are the underlying mechanisms? We explain it using the argument from Schubert et al. (1979a), who stress the role of the pressure field. The central idea is that the pressure gradient force propels the air overturning, transferring the warm air downward to the top of the surface stable layer. The warm air mass at the top of the surface stable layer is eventually delivered to the surface by preexisting TKE (e.g., mechanically driven). The effect of pressure transport can be more clearly illustrated by the $\overline{w'p'}$ profile of the WADV experiment (Fig. 10). The $\overline{w'p'}$ is negative in the subcloud layer for both updrafts and downdrafts. This suggests that air rises in low pressure regions and sinks in high pressure regions, typical for pressure-driven air overturning. The negative $\overline{w'p'}$ at the cloud base suggests that the cloud layer does work on the subcloud layer, pumping up the subcloud air, completing the circulation. This process is consistent with the idea of boundary layer energetics. As the boundary layer is stabilized by the warm-air advection, the turbulence generated from the cloud-top radiative cooling must work against the stability to mix the boundary layer. This is a process that converts turbulent energy to the potential energy of the environment. Such an energy conversion is realized by the descending of warm air, propelled by the pressure gradient.

Brought to you by PRINCETON UNIVERSITY LIBRARY | Unauthenticated | Downloaded 07/29/22 03:00 PM UTC

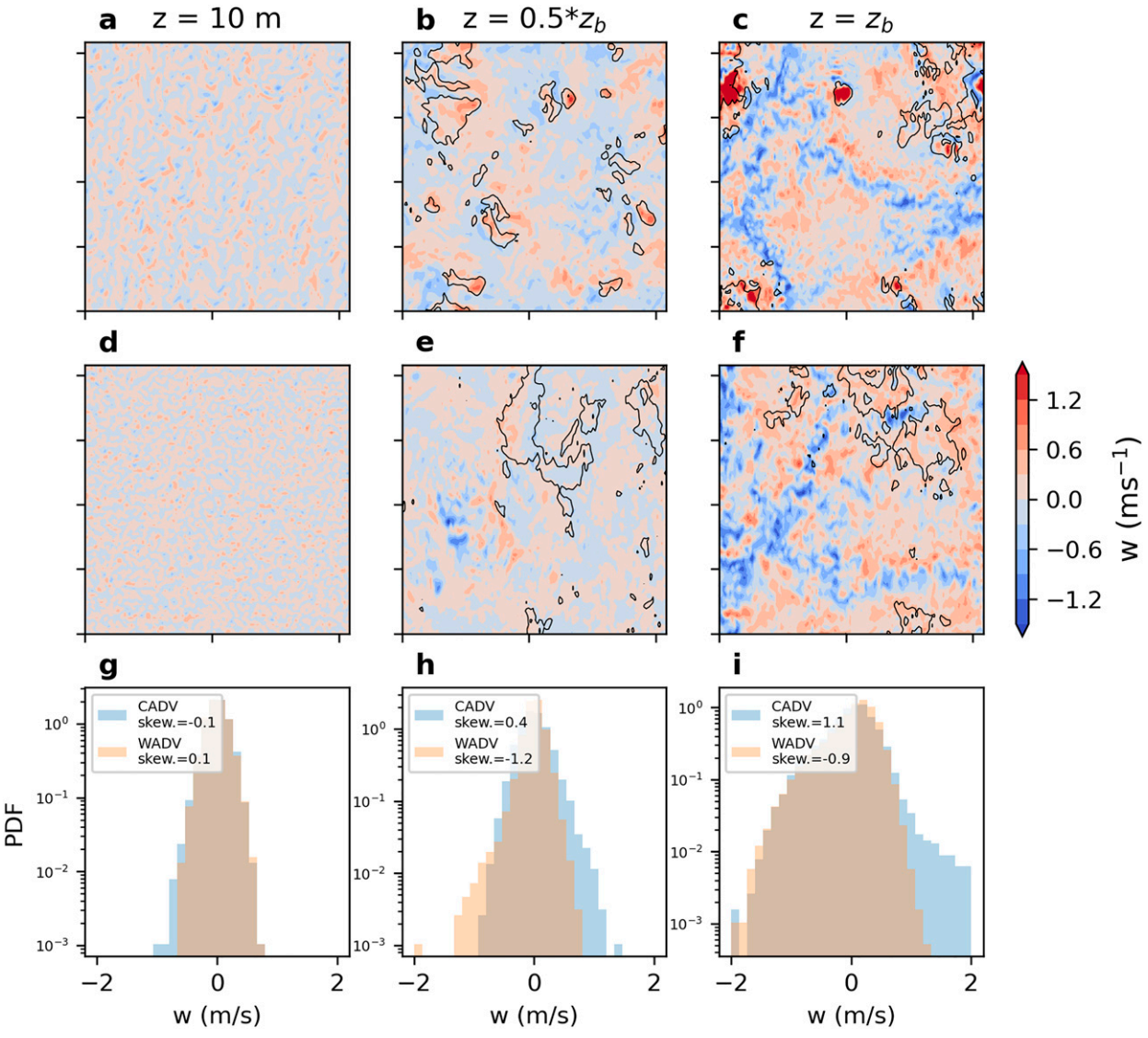


FIG. 8. Vertical velocity field at (left) $z = 10$ m, (center) $z = 0.5z_b$, and (right) $z = z_b$ for the (a)–(c) CADV and (d)–(f) WADV. (g)–(i) The probability distribution functions of the vertical velocity for the two experiments. In (b), (c), (e), and (f), black contours correspond to the top 10% q_t in each horizontal layer.

c. *On the formation of double-layer stratiform clouds*

From observations, under warm-air advection conditions, often found are double-layer stratiform clouds, with the upper layer capped by the major temperature inversion and the lower layer close to the surface, often manifested as fog (Zheng et al. 2020; M. Smalley and S. Klein 2020, personal communications). It is, thus, important to understand why our WADV experiment does not develop a stratus near surface.

A hypothesis that naturally arises is that, in the WADV run, the near-surface temperature inversion is not sufficiently strong to sustain high humidity (by trapping water vapor within it). To test this hypothesis, we run additional simulations by altering the forcing parameters for the WADV. First, we double the Tadv from 2.6 to 5.2 K day^{-1}, denoted as "WADV5.2." The expectation is that if the SST cools rapidly enough, the near-surface inversion may be strong enough to form fogs. Second, we decrease the large-scale divergence from 5×10^{-6} to 3×10^{-6}, denoted as "WADV Div3." We expect that, for weaker subsidence, the boundary layer deepens more rapidly, enhancing the warming of the upper boundary layer, which strengthens the near-surface temperature inversion.

Figure 11 shows the cross sections of cloudiness of the two experiments. A double-layer stratiform cloud emerges in the WADV Div3, but not in WADV5.2 (only a tiny number of small clouds below the Sc deck). The bottom panel of Fig. 11 shows the sounding at $t = 30$ h. The filled circles mark the

Brought to you by PRINCETON UNIVERSITY LIBRARY | Unauthenticated | Downloaded 07/29/22 03:00 PM UTC

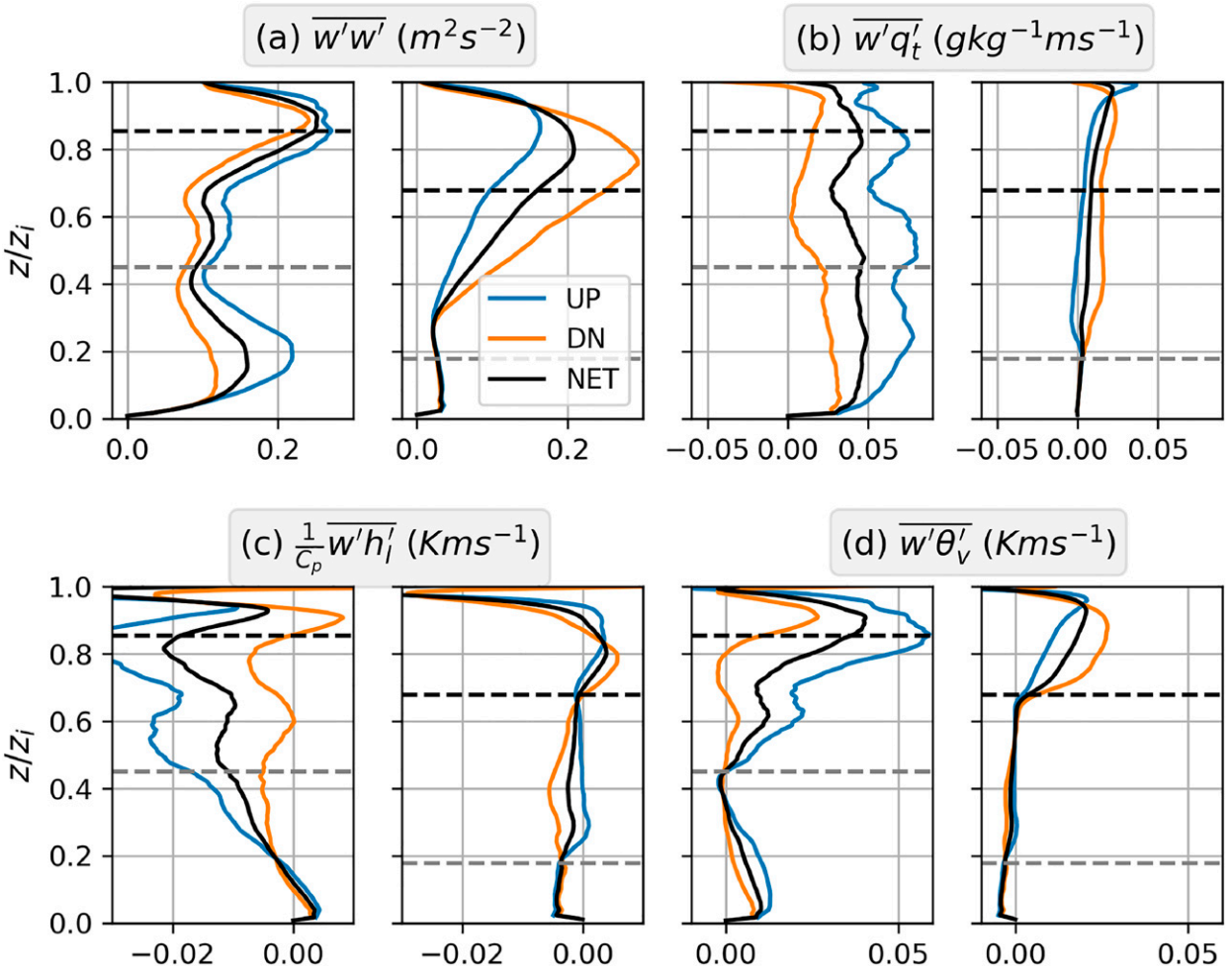


FIG. 9. Vertical profiles of (a) resolved vertical velocity variance, (b) moisture flux, (c) heat flux, and (d) buoyancy flux of updrafts (blue) and downdrafts (orange) for (left) CADV and (right) WADV. Horizontal black and gray dashed lines mark the base heights of stratocumulus decks and LCL, respectively.

heights of the near-surface temperature inversion, z_{li}, determined as the level of the local maxima of liquid water potential temperature variance (Yamaguchi and Randall 2008). We find that both new experiments generate stronger near-surface inversions than the WADV (Fig. 11c), consistent with our expectations. However, a strong temperature inversion does not necessarily increase the q_t: relative to WADV, the q_t within the inversion is higher in WADV Div3, but lower in WADV5.2 (Fig. 11d). For this reason, the WADV5.2 does not develop enough high RH to form a cloud (Fig. 11e).

To understand what drives the difference in the q_t, we consider the atmosphere from the surface to the z_{li} as a bulk layer and take the $\overline{w'q_t'}$ at the top and bottom, denoted as $(\overline{w'q_t'})_{\text{top}}$ and $(\overline{w'q_t'})_{\text{bot}}$, respectively (Figs. 12a,b). Their difference divided by the z_{li} yields the net moistening rate of the near-surface layer (Fig. 12c). We found considerably smaller $(\overline{w'q_t'})_{\text{bot}}$ in WADV5.2 than the other two runs (Fig. 12b), suggesting that the downward decrease in humidity is the primary reason for its greater drying (Figs. 12c and 11d). The negative $(\overline{w'q_t'})_{\text{bot}}$ is driven by the more negative q_t gradient across the surface, namely, $q^*_{\text{sfc}} - q_{\text{air}}$, where the q^*_{sfc} is the saturation q_t of the SST and q_{air} is the q_t of the overlying air (Fig. 12d). The more negative $q^*_{\text{sfc}} - q_{\text{air}r}$ is fundamentally constrained by the Clausius–Clapeyron relation. Unlike the WADV5.2, the WADV Div 3 does not experience any changes in the $(\overline{w'q_t'})_{\text{bot}}$ compared with the WADV. Instead, the $(\overline{w'q_t'})_{\text{top}}$ becomes markedly smaller than that of the WADV.[2] This means less upward loss of moisture, thereby elevating the q_t relative to the WADV.

In summary, weaker subsidence favors the emergence of double-layer stratiform clouds because weaker subsidence allows for more rapid boundary layer deepening, which

[2] The smaller $(\overline{w'q_t'})_{\text{top}}$ is driven by the stronger near-surface temperature inversion at WADV Div3 (Fig. 10a), which inhibits the vertical exchange of moisture between the bottom and upper boundary layer.

Brought to you by PRINCETON UNIVERSITY LIBRARY | Unauthenticated | Downloaded 07/29/22 03:00 PM UTC

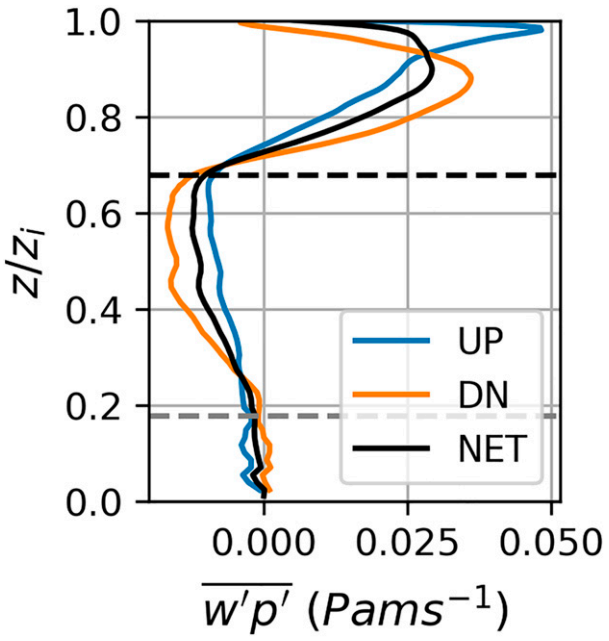


FIG. 10. Vertical profiles of $\overline{w'p'}$ at $t = 30$ h in WADV.

warms the upper boundary layer, enhancing the near-surface temperature inversion. The stronger near-surface temperature inversion traps the moisture within, eventually elevating the RH to unity. Stronger warm advection (i.e., more rapid sea surface cooling) does not necessarily favor the formation of such secondary stratus because a cooler sea surface facilitates the downward transport of moisture from the atmosphere into the sea. This acts to dry the near-surface air, preventing the formation of clouds. This argument may become less tenable when the surface cooling is strong enough to significantly change the transport behavior.

4. Summary

We have investigated the response of a stratocumulus-topped boundary layer (STBL) to a cooling sea surface by using idealized large-eddy simulations. The decreasing sea surface temperature mimics the influence of low-level warm-air advection (WADV). In addition to characterizing the basic turbulence structure of the boundary layer in WADV, we are particularly interested in testing an unproven hypothesis: an unambiguous decoupling between stratocumulus clouds and the surface can be achieved in WADV flow, but not in cold advection (CADV) flow because the latter favors cumulus-induced coupling while the former does not (Zheng and Li 2019; Zheng et al. 2020). To examine this argument, we investigate the decoupling physics of an STBL experiencing WADV and compare the results with that in CADV. We found the followings:

(i) An STBL tends to become stably stratified in both WADV and CADV conditions, but their driving mechanism is dramatically different. The stratification in CADV is caused by the enhanced entrainment warming (i.e., the "deepening-warming" theory by Bretherton and Wyant 1997) whereas, in WADV, it is driven by cooling of the bottom boundary layer due to radiative cooling and loss of heat to the sea surface via turbulent transport. The difference in the driving mechanism constitutes a decoupling dipole: top-warming driven versus bottom-cooling driven.

(ii) The surface cooling in the WADV condition causes a temperature inversion in the lower boundary layer. Above the inversion is a well-mixed cloud-containing layer whose convection is driven by the cloud-top radiative cooling. This is different from the temperature structure in CADV that has two well-mixed layers separated by a conditionally unstable layer.

(iii) The difference in the boundary layer thermodynamics between WADV and CADV significantly alters the turbulence and cloud regimes. Unlike the emergence of cumulus-coupled stratocumulus in CADV, the WADV simulation manifests a single stratocumulus deck that is persistent, horizontally homogeneous, relatively quiet, and unambiguously decoupled from the moisture source of the sea surface. Such a cloud pattern is a consequence of a lack of surface fluxes, leaving the cloud-top cooling the only driver of convection.

(iv) Due to the lack of surface fluxes, the buoyancy flux profile in WADV manifests a dipole pattern: positive in the cloud layer and weakly negative in the subcloud layer. This, in combination with the profile of the pressure covariation with the vertical velocity, dictates that the cloud layer does work to the subcloud layer to pump up the air, maintaining the convective circulation. Such a cloud-containing mixed layer, however, cannot extend down to the surface because of the strong near-surface inversion sustained by the surface cooling. This is, again, in contrast to the convective circulation in CADV that is not only driven by cloud-top cooling but also surface heating that propels strong updrafts responsible for the bulk of the heat and moisture transports.

(v) A secondary stratiform cloud (or fog) can form in the lower boundary layer in WADV if the large-scale subsidence weakens. The mechanism is that the STBL deepens more rapidly if the subsidence is weaker. The intrusion of the STBL into warmer free atmosphere weakens the buoyancy jump across the boundary layer top, enhancing the entrainment of overlying warm air into the boundary layer. The warming enhances the temperature gradient between the warm boundary layer and the cold ocean. This strengthens the near-surface temperature inversion, trapping more water vapor within the layer, raising the relative humidity to unity. Interestingly, increasing the cooling rate of sea surface temperature does not necessarily cause the formation of the fog. The reason is that colder sea surface enhances the negative moisture gradient between the air in contact with the sea surface and the overlying air. This causes a more rapid loss of moisture from the near-surface air to the sea, thereby suppressing the fog formation.

Brought to you by PRINCETON UNIVERSITY LIBRARY | Unauthenticated | Downloaded 07/29/22 03:00 PM UTC

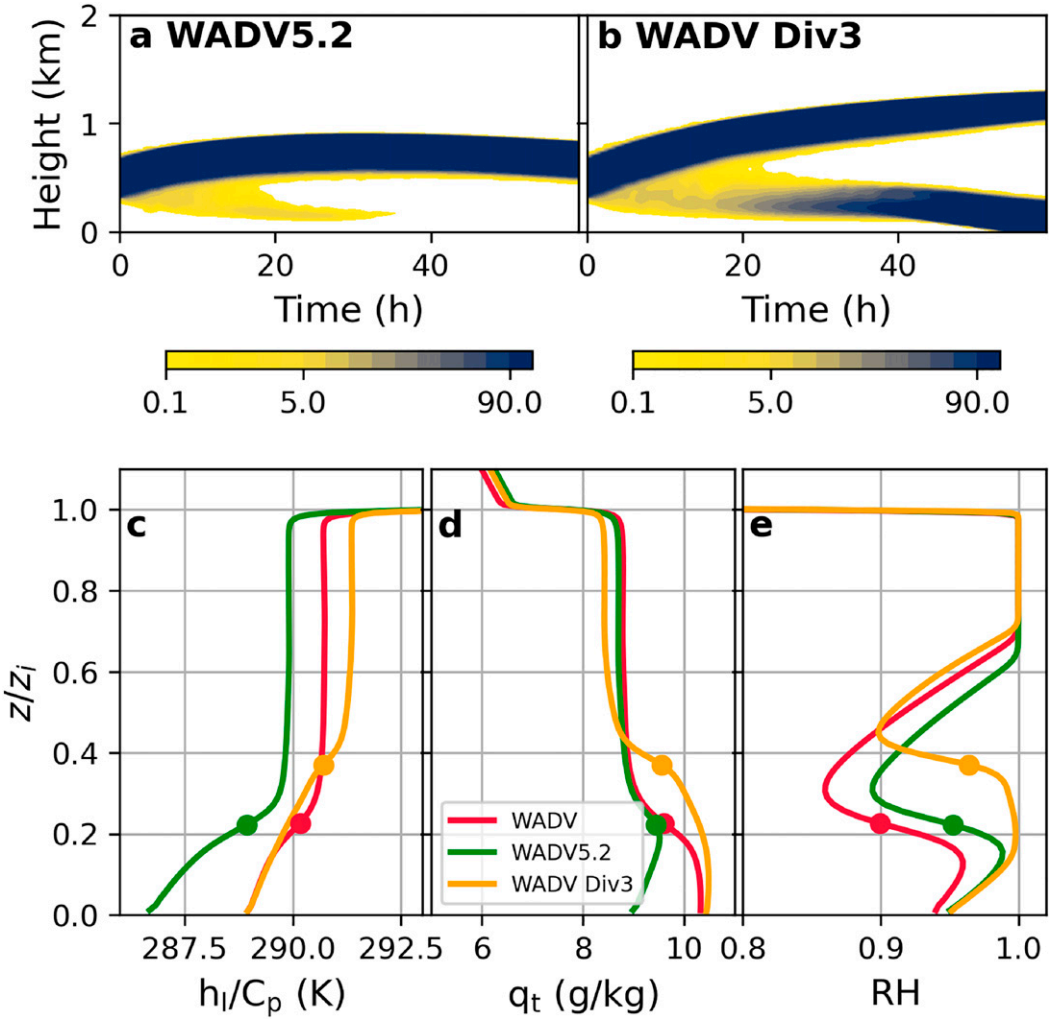


FIG. 11. Time–height plots of cloud fraction for (a) WADV5.2 and (b) WADV Div3, and vertical profiles of (c) h_l/C_p, (d) q_t, and (e) relative humidity for the WADV, WADV5.2, and WADV Div3. The solid dots mark the z_{li}.

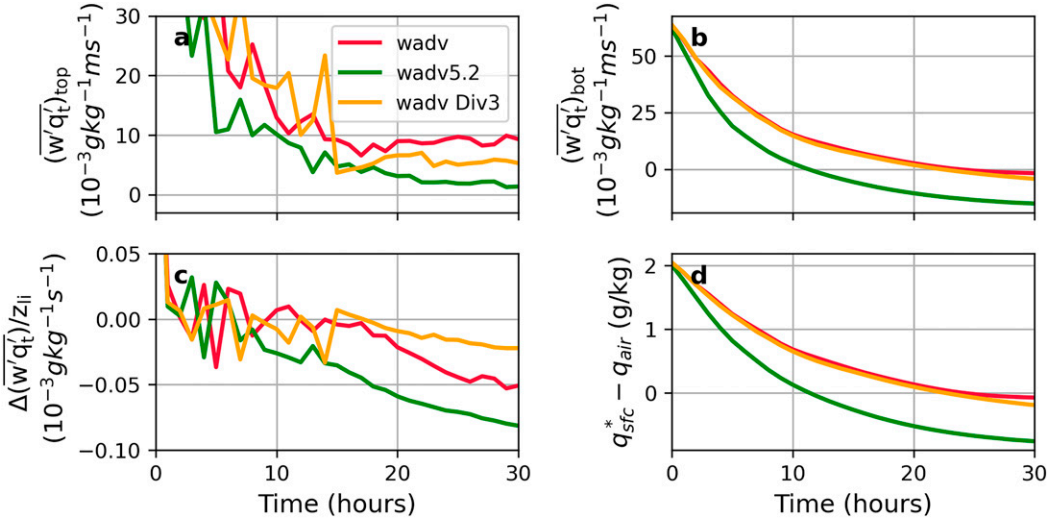


FIG. 12. Time series of (a) $\overline{(w'q_t')}_{\text{top}}$, (b) $\overline{(w'q_t')}_{\text{bot}}$, (c) $\left[\overline{(w'q_t')}_{\text{top}} - \overline{(w'q_t')}_{\text{bot}}\right]/z_{li}$, and (d) $q^*_{\text{sfc}} - q_{\text{air}}$ for the three WADV runs.

Brought to you by PRINCETON UNIVERSITY LIBRARY | Unauthenticated | Downloaded 07/29/22 03:00 PM UTC

Acknowledgments. This study is supported by the Department of Energy (DOE) Atmospheric System Research program (DE-SC0018996). S.-S. Lee is also supported by the National Research Foundation of Korea (NRF) grant funded by the South Korean government (MSIT) (Grant NRF2020R1A2C1003215). The authors acknowledge the University of Maryland supercomputing resources (http://hpcc.umd.edu) made available for conducting the research reported in this paper. We thank Marat Khairoutdinov for maintaining the SAM code and Peter Blossey for helping with setting up the ASTEX case. We thank three anonymous reviewers for their constructive comments. The SAM model code is available at http://rossby.msrc.sunysb.edu/~marat/SAM.html. The simulation data are available at https://doi.org/10.5281/zenodo.5548436. The codes used to reproduce the results can be obtained from https://github.com/youtongzheng/Zheng_2021_JAS_WADV_part1.

REFERENCES

Agee, E. M., 1987: Mesoscale cellular convection over the oceans. *Dyn. Atmos. Oceans*, **10**, 317–341, https://doi.org/10.1016/0377-0265(87)90023-6.

Albrecht, B. A., C. S. Bretherton, D. Johnson, W. H. Schubert, and A. S. Frisch, 1995: The Atlantic Stratocumulus Transition Experiment—ASTEX. *Bull. Amer. Meteor. Soc.*, **76**, 889–904, https://doi.org/10.1175/1520-0477(1995)076<0889:TASTE>2.0.CO;2.

Bjerknes, J., 1938: Saturated-adiabatic ascent of air through dry-adiabatically descending environment. *Quart. J. Roy. Meteor. Soc.*, **64**, 325–30.

Bretherton, C. S., 1997: Convection in stratocumulus-topped atmospheric boundary layers. *The Physics and Parameterization of Moist Atmospheric Convection*, Springer, 127–142.

——, and M. C. Wyant, 1997: Moisture transport, lower-tropospheric stability, and decoupling of cloud-topped boundary layers. *J. Atmos. Sci.*, **54**, 148–167, https://doi.org/10.1175/1520-0469(1997)054<0148:MTLTSA>2.0.CO;2.

——, and P. N. Blossey, 2014: Low cloud reduction in a greenhouse-warmed climate: Results from Lagrangian LES of a subtropical marine cloudiness transition. *J. Adv. Model. Earth Syst.*, **6**, 91–114, https://doi.org/10.1002/2013MS000250.

——, J. Uchida, and P. N. Blossey, 2010: Slow manifolds and multiple equilibria in stratocumulus-capped boundary layers. *J. Adv. Model. Earth Syst.*, **2**, 14, https://doi.org/10.3894/JAMES.2010.2.14.

Caldwell, P., and C. S. Bretherton, 2009: Response of a subtropical stratocumulus-capped mixed layer to climate and aerosol changes. *J. Climate*, **22**, 20–38, https://doi.org/10.1175/2008JCLI1967.1.

——, ——, and R. Wood, 2005: Mixed-layer budget analysis of the diurnal cycle of entrainment in southeast Pacific stratocumulus. *J. Atmos. Sci.*, **62**, 3775–3791, https://doi.org/10.1175/JAS3561.1.

Edwards, J. M., 2009: Radiative processes in the stable boundary layer: Part I. Radiative aspects. *Bound.-Layer Meteor.*, **131**, 105–126, https://doi.org/10.1007/s10546-009-9364-8.

Fletcher, J. K., S. Mason, and C. Jakob, 2016: A climatology of clouds in marine cold air outbreaks in both hemispheres. *J. Climate*, **29**, 6677–6692, https://doi.org/10.1175/JCLI-D-15-0783.1.

Goren, T., D. Rosenfeld, O. Sourdeval, and J. Quaas, 2018: Satellite observations of precipitating marine stratocumulus show greater cloud fraction for decoupled clouds in comparison to coupled clouds. *Geophys. Res. Lett.*, **45**, 5126–5134, https://doi.org/10.1029/2018GL078122.

Hahn, C. J., and S. G. Warren, 2007: A gridded climatology of clouds over land (1971–96) and ocean (1954–97) from surface observations worldwide. CDIAC Rep. ORNL/CDIAC-153, 71 pp., https://doi.org/10.3334/CDIAC/cli.ndp026e.

Hartmann, D. L., M. E. Ockert-Bell, and M. L. Michelsen, 1992: The effect of cloud type on Earth's energy balance: Global analysis. *J. Climate*, **5**, 1281–1304, https://doi.org/10.1175/1520-0442(1992)005<1281:TEOCTO>2.0.CO;2.

Holton, J. R., 1973: An introduction to dynamic meteorology. *Amer. J. Phys.*, **41**, 752–754, https://doi.org/10.1119/1.1987371.

Iacono, M. J., J. S. Delamere, E. J. Mlawer, M. W. Shephard, S. A. Clough, and W. D. Collins, 2008: Radiative forcing by long-lived greenhouse gases: Calculations with the AER radiative transfer models. *J. Geophys. Res.*, **113**, D13103, https://doi.org/10.1029/2008JD009944.

Jones, C., C. Bretherton, and P. Blossey, 2014: Fast stratocumulus time scale in mixed layer model and large eddy simulation. *J. Adv. Model. Earth Syst.*, **6**, 206–222, https://doi.org/10.1002/2013MS000289.

Khairoutdinov, M., and Y. Kogan, 2000: A new cloud physics parameterization in a large-eddy simulation model of marine stratocumulus. *Mon. Wea. Rev.*, **128**, 229–243, https://doi.org/10.1175/1520-0493(2000)128<0229:ANCPPI>2.0.CO;2.

——, and D. A. Randall, 2003: Cloud resolving modeling of the ARM summer 1997 IOP: Model formulation, results, uncertainties, and sensitivities. *J. Atmos. Sci.*, **60**, 607–625, https://doi.org/10.1175/1520-0469(2003)060<0607:CRMOTA>2.0.CO;2.

Klein, S. A., A. Hall, J. R. Norris, and R. Pincus, 2017: Low-cloud feedbacks from cloud-controlling factors: A review. *Shallow Clouds, Water Vapor, Circulation, and Climate Sensitivity*, Springer, 135–157.

Lilly, D. K., 1968: Models of cloud-topped mixed layers under a strong inversion. *Quart. J. Roy. Meteor. Soc.*, **94**, 292–309, https://doi.org/10.1002/qj.49709440106.

Mahrt, L., 2014: Stably stratified atmospheric boundary layers. *Annu. Rev. Fluid Mech.*, **46**, 23–45, https://doi.org/10.1146/annurev-fluid-010313-141354.

Mellado, J. P., 2017: Cloud-top entrainment in stratocumulus clouds. *Annu. Rev. Fluid Mech.*, **49**, 145–169, https://doi.org/10.1146/annurev-fluid-010816-060231.

——, C. S. Bretherton, B. Stevens, and M. C. Wyant, 2018: DNS and LES for simulating stratocumulus: Better together. *J. Adv. Model. Earth Syst.*, **10**, 1421–1438, https://doi.org/10.1029/2018MS001312.

Miller, M. A., and B. A. Albrecht, 1995: Surface-based observations of mesoscale cumulus–stratocumulus interaction during ASTEX. *J. Atmos. Sci.*, **52**, 2809–2826, https://doi.org/10.1175/1520-0469(1995)052<2809:SBOOMC>2.0.CO;2.

Moeng, C.-H., and R. Rotunno, 1990: Vertical-velocity skewness in the buoyancy-driven boundary layer. *J. Atmos. Sci.*, **47**, 1149–1162, https://doi.org/10.1175/1520-0469(1990)047<1149:VVSITB>2.0.CO;2.

Myers, T. A., and J. R. Norris, 2015: On the relationships between subtropical clouds and meteorology in observations and CMIP3 and CMIP5 models. *J. Climate*, **28**, 2945–2967, https://doi.org/10.1175/JCLI-D-14-00475.1.

Naud, C. M., J. F. Booth, A. Protat, K. Lamer, R. Marchand, and G. M. McFarquhar, 2020: Boundary layer cloud controlling

Brought to you by PRINCETON UNIVERSITY LIBRARY | Unauthenticated | Downloaded 07/29/22 03:00 PM UTC

factors in the midlatitudes: Southern versus northern ocean clouds. *2020 AGU Fall Meeting*, Virtual, Amer. Geophys. Union, Abstract A195-02.

Nicholls, S., 1984: The dynamics of stratocumulus: Aircraft observations and comparisons with a mixed layer model. *Quart. J. Roy. Meteor. Soc.*, **110**, 783–820, https://doi.org/10.1002/qj.49711046603.

——, and J. Leighton, 1986: An observational study of the structure of stratiform cloud sheets: Part I. Structure. *Quart. J. Roy. Meteor. Soc.*, **112**, 431–460, https://doi.org/10.1002/qj.49711247209.

Norris, J. R., and S. A. Klein, 2000: Low cloud type over the ocean from surface observations. Part III: Relationship to vertical motion and the regional surface synoptic environment. *J. Climate*, **13**, 245–256, https://doi.org/10.1175/1520-0442(2000)013<0245:LCTOTO>2.0.CO;2.

——, and S. F. Iacobellis, 2005: North Pacific cloud feedbacks inferred from synoptic-scale dynamic and thermodynamic relationships. *J. Climate*, **18**, 4862–4878, https://doi.org/10.1175/JCLI3558.1.

Petty, G. W., 2006: *A First Course in Atmospheric Radiation.* 2nd ed. Sundog Publishing, 459 pp.

Romps, D. M., 2017: Exact expression for the lifting condensation level. *J. Atmos. Sci.*, **74**, 3891–3900, https://doi.org/10.1175/JAS-D-17-0102.1.

Sandu, I., and B. Stevens, 2011: On the factors modulating the stratocumulus to cumulus transitions. *J. Atmos. Sci.*, **68**, 1865–1881, https://doi.org/10.1175/2011JAS3614.1.

Schubert, W. H., J. S. Wakefield, E. J. Steiner, and S. K. Cox, 1979a: Marine stratocumulus convection. Part I: Governing equations and horizontally homogeneous solutions. *J. Atmos. Sci.*, **36**, 1286–1307, https://doi.org/10.1175/1520-0469(1979)036<1286:MSCPIG>2.0.CO;2.

——, ——, ——, and ——, 1979b: Marine stratocumulus convection. Part II: Horizontally inhomogeneous solutions. *J. Atmos. Sci.*, **36**, 1308–1324, https://doi.org/10.1175/1520-0469(1979)036<1308:MSCPIH>2.0.CO;2.

Scott, R. C., T. A. Myers, J. R. Norris, M. D. Zelinka, S. A. Klein, M. Sun, and D. R. Doelling, 2020: Observed sensitivity of low cloud radiative effects to meteorological perturbations over the global oceans. *J. Climate*, **33**, 7717–7734, https://doi.org/10.1175/JCLI-D-19-1028.1.

Smolarkiewicz, P. K., and W. W. Grabowski, 1990: The multidimensional positive definite advection transport algorithm: Nonoscillatory option. *J. Comput. Phys.*, **86**, 355–375, https://doi.org/10.1016/0021-9991(90)90105-A.

Stevens, B., 2006: Bulk boundary-layer concepts for simplified models of tropical dynamics. *Theor. Comput. Fluid Dyn.*, **20**, 279–304, https://doi.org/10.1007/s00162-006-0032-z.

——, W. R. Cotton, G. Feingold, and C.-H. Moeng, 1998: Large-eddy simulations of strongly precipitating, shallow, stratocumulus-topped boundary layers. *J. Atmos. Sci.*, **55**, 3616–3638, https://doi.org/10.1175/1520-0469(1998)055<3616:LESOSP>2.0.CO;2.

Uchida, J., C. Bretherton, and P. Blossey, 2010: The sensitivity of stratocumulus-capped mixed layers to cloud droplet concentration: Do LES and mixed-layer models agree? *Atmos. Chem. Phys.*, **10**, 4097–4109, https://doi.org/10.5194/acp-10-4097-2010.

Van der Dussen, J., and Coauthors, 2013: The GASS/EUCLIPSE model intercomparison of the stratocumulus transition as observed during ASTEX: LES results. *J. Adv. Model. Earth Syst.*, **5**, 483–499, https://doi.org/10.1002/jame.20033.

Wakefield, J. S., and W. H. Schubert, 1981: Mixed-layer mode simulation of eastern North Pacific stratocumulus. *Mon. Wea. Rev.*, **109**, 1952–1968, https://doi.org/10.1175/1520-0493(1981)109<1952:MLMSOE>2.0.CO;2.

Wall, C. J., D. L. Hartmann, and P.-L. Ma, 2017: Instantaneous linkages between clouds and large-scale meteorology over the Southern Ocean in observations and a climate model. *J. Climate*, **30**, 9455–9474, https://doi.org/10.1175/JCLI-D-17-0156.1.

Wood, R., 2007: Cancellation of aerosol indirect effects in marine stratocumulus through cloud thinning. *J. Atmos. Sci.*, **64**, 2657–2669, https://doi.org/10.1175/JAS3942.1.

——, 2012: Stratocumulus clouds. *Mon. Wea. Rev.*, **140**, 2373–2423, https://doi.org/10.1175/MWR-D-11-00121.1.

Wyngaard, J., 1987: A physical mechanism for the asymmetry in top-down and bottom-up diffusion. *J. Atmos. Sci.*, **44**, 1083–1087, https://doi.org/10.1175/1520-0469(1987)044<1083:APMFTA>2.0.CO;2.

Yamaguchi, T., and D. A. Randall, 2008: Large-eddy simulation of evaporatively driven entrainment in cloud-topped mixed layers. *J. Atmos. Sci.*, **65**, 1481–1504, https://doi.org/10.1175/2007JAS2438.1.

Zhang, Y., B. Stevens, and M. Ghil, 2005: On the diurnal cycle and susceptibility to aerosol concentration in a stratocumulus-topped mixed layer. *Quart. J. Roy. Meteor. Soc.*, **131**, 1567–1583, https://doi.org/10.1256/qj.04.103.

Zheng, Y., and Z. Li, 2019: Episodes of warm-air advection causing cloud-surface decoupling during the MARCUS. *J. Geophys. Res. Atmos.*, **124**, 12 227–12 243, https://doi.org/10.1029/2019JD030835.

——, D. Rosenfeld, and, Z. Li, 2018: The relationships between cloud top radiative cooling rates, surface latent heat fluxes, and cloud-base heights in marine stratocumulus. *J. Geophys. Res. Atmos.*, **123**, 11 678–11 690, https://doi.org/10.1029/2018JD028579.

——, ——, and ——, 2020: A more general paradigm for understanding the decoupling of stratocumulus-topped boundary layers: The importance of horizontal temperature advection. *Geophys. Res. Lett.*, **47**, e2020GL087697, https://doi.org/10.1029/2020GL087697.

——, H. Zhang, and Z. Li, 2021: Role of surface latent heat flux in shallow cloud transitions: A mechanism-denial LES study. *J. Atmos. Sci.*, **78**, 2709–2723, https://doi.org/10.1175/JAS-D-20-0381.1.

Brought to you by PRINCETON UNIVERSITY LIBRARY | Unauthenticated | Downloaded 07/29/22 03:00 PM UTC